J Nanopart Res (2013) 15:1706
DOI 10.1007/s11051-013-1706-2

RESEARCH PAPER

Physical stability, biocompatibility and potential use of hybrid iron oxide-gold nanoparticles as drug carriers

Christopher M. Barnett · Mariana Gueorguieva · Martin R. Lees · David J. McGarvey · Clare Hoskins

Received: 9 February 2013 / Accepted: 6 May 2013

Abstract Hybrid nanoparticles (HNPs) such as iron oxide-gold nanoparticles are currently being exploited for their potential application in image-guided therapies. However, little investigation has been carried out into their physical or chemical stability and potential cytotoxicity in biological systems. Here, we determine the HNPs physical stability over 6 months and chemical stability in physiological conditions, and estimate the biological activity of uncoated and poly(ethylene glycol) coated nanoparticles on human pancreatic adenocarcinoma (BxPC-3) and differentiated human monocyte cells (U937). The potential of these HNPs to act as drug carrier vehicles was determined using the model drug 6-Thioguanine (6-TG). The data showed that the HNPs maintained their structural integrity both physically and chemically throughout the duration of the studies. In addition, negligible cytotoxicity or free radical production was observed in the cell lines tested. The 6-TG was successfully conjugated; with a ratio of 3:1:10 Fe:Au:6-TG (wt:wt:wt). After incubation with BxPC-3 cells, enhanced cellular uptake was reported with the 6-TG-conjugated HNPs compared with free drug along with a 10-fold decrease in IC_{50}. This exciting data highlights the potential of HNPs for use in image-guided drug delivery.

Keywords Hybrid nanoparticle · Magnetic nanoparticle · Gold nano-shell · Stability · Biocompatibility · Drug delivery

C. M. Barnett
School of Pharmacy, Keele University, Keele ST5 5BG, UK

M. Gueorguieva
Institute of Medical Science and Technology, University of Dundee, Dundee DD2 1FD, UK

M. R. Lees
Physics Department, University of Warwick, Coventry CV4 7AL, UK

D. J. McGarvey
Lennard-Jones Laboratories, School of Physical and Geographical Sciences, Keele University, Keele ST5 5BG, UK

C. Hoskins (✉)
Institute for Science and Technology in Medicine, Keele University, Keele ST5 5BG, UK
e-mail: c.hoskins@keele.ac.uk

Introduction

Recently, hybrid nanoparticles (HNPs) composed of iron oxide cores surrounded by a gold coating have emerged as potential multifunctional agents for image-guided drug delivery (Ji et al. 2007; Hoskins et al. 2012a). In order for these HNPs to be used for biomedical applications, first their physical stability and safety profile must be determined. Safety concerns over the use of iron oxide nanoparticles in humans has increased in recent years, with the lack of in-depth

Published online: 15 May 2013

understanding of the fate of these nanoparticles and their effect on their surroundings in vivo (Fadeel and Garcia-Bennett 2010). These concerns culminated in the withdrawal of the clinically used magnetic resonance imaging (MRI) contrast agent Feridex® from use in humans in the UK (Hoskins et al. 2012a). Therefore, before any biomedical application of said metallic nanoparticles can be achieved, they need to undergo suitable testing to ensure appropriate safety levels are met. Hence, with the increasing potential of HNPs being realised, the current priority lies in determining the bio-safety of these particles. It has previously been hypothesized that the gold coating provides a rigid shield protecting the external environment from the inherent toxicity of the iron oxide core (Barnett et al. 2012). Furthermore, the rigid nature of the gold coating should be more effective than traditionally used polymers in protecting the iron oxide core from degradation in physiological conditions (Barnett et al. 2012). A reduction in degradation will limit free radical production in vivo and hence, increase the biocompatibility of the system (Lu et al. 2007; Hoskins et al. 2012b). Our group previously reported HNPs showed promising physical properties for application in biomedicine (Barnett et al. 2012). However, their chemical stability and biological activity had not yet been determined. In this study, HNPs composed of iron oxide with a poly(ethylenimine) (PEI) intermediate and subsequent gold coating (70 nm) will be investigated (Barnett et al. 2012). Namely, the chemical and physical stability of these particles will be studied along with their safety profile in vitro.

It has been shown that further engineering on the surface of the gold shell would result in greater cellular internalisation, for example, with poly(ethylene glycol) (PEG)—a biocompatible polymer approved for use in humans (Vila et al. 2004). In fact, PEG molecules have been used extensively in the coating of inorganic nanoparticles (Peng et al. 2008; Józejczak and Skumiel 2011; Manson et al. 2011). PEGylation of nanoparticulates has been shown to promote cellular uptake without causing undesirable toxic side effects (Vila et al. 2004). In order to effectively understand the potential toxicity issues of these HNPs, it is vital for transfection to be achieved. Hence, nanoparticles will be PEG-coated, and cellular internalisation, viability and response assays conducted using both the uncoated and PEGylated HNPs in human pancreatic adenocarcinoma (BxPC-3) and differentiated human monocyte (U937) cell lines. It is understood that acute toxicity arising from nanoparticulate structures is largely attributed to their surface chemistry (Buzea et al. 2007; Albanese et al. 2012). However, in the case of Feridex®, which was coated with clinically approved dextran, it was the flexible polymer not providing adequate protection from the toxic core, which is thought to have led to toxicity and ultimately its withdrawal (Hoskins et al. 2012a). With this in mind, PEG is used here largely to aid in the transfection of the HNPs and not to mask their potential cytotoxicity (Mishra et al. 2004).

In our previous study, the physical properties of HNPs were realised in terms of their contrast ability and thermal manipulation (Hoskins et al. 2012a; Barnett et al. 2012). However, their ability to act as drug carrier vehicles was not investigated. Magnetic iron oxide nanoparticles have previously been exploited for the ability to carry pharmaceutical cargo (Dobson 2006; Arruebo et al. 2007; Sun et al. 2008; Chatterjee et al. 2011). Recently, a study has shown the potential of HNPs for drug delivery in vitro (Wagstaff et al. 2012). Here, the anticancer agent cisplatin was used to show the potential of HNPs as drug carriers in localised magnetic fields. Wagstaff and colleagues coupled the cisplatin to a thiolated PEG which was ultimately conjugated to the HNP surface. The drug conjugate achieved drug loading of 7.9×10^{-4} mol of platinum per grams of gold. The cytotoxic potential of the HNP-drug conjugates was studied in vitro on human ovarian cancer (A2780) and cisplatin resistant (A2780/cp70) cell lines. This study showed that the HNP-drug conjugate decreased the IC_{50} up to 110-fold compared to the free drug (Wagstaff et al. 2012).

To elucidate the potential of our HNPs as drug vehicles the model drug 6-thioguanine (6-TG) will be used. 6-TG is an antitumour agent currently used clinically in the treatment of leukaemia (Lancaster et al. 2001). 6-TG belongs to the thiopurine series of compounds which are renowned for their immunosuppressant properties and are commonly used in organ transplants to reduce rejection of new tissue, and also in the treatment of Crohn's disease (Zaza et al. 2010). 6-TG will be conjugated onto the HNP surface via dative covalent bonding and the drug conjugation capacity will be determined. Furthermore, in vitro studies pertaining to drug uptake and the cytotoxic

effect of the HNP-drug conjugates on BxPC-3 cells will be evaluated.

Materials and methods

All chemicals unless otherwise stated were purchased from Sigma-Aldrich (UK).

Synthesis and PEGylation of hybrid nanoparticles

Particles of 70 nm diameter were synthesised and characterised as previously reported (Barnett et al. 2012). In this study, gold coated iron oxide nanoparticles coated containing a poly(ethylenimine) (PEI) intermediate layer were used (previously described as Fe_3O_{4S}–PEI–Au_{COAT}), and shall be referred to herein as hybrid nanoparticles (HNPs). HNP's (2 mL) were stirred with *O*-[2-(3-Mercaptopropionyl amino) ethyl]-*O*′-methylpolyethylene glycol (PEG-Thiol, 1 mg mL^{-1}) for 2 h at 60 °C. The HNPs were washed five times with deionised water and magnetically separated from solution. The resultant particles (5 mg) were resuspended in 5 mL deionised water.

Characterisation of PEGylated HNPs

Fourier transform infrared (FTIR) and elemental analysis were used to determine if the PEG coating had been successful. The PEGylated HNPs (HNP-PEG) were freeze-dried prior to FTIR spectroscopy. The dry powder was measured using a diamond tipped attenuated total reflectance attachment (Nicolette IS50, Thermo-Fisher UK). The samples were scanned 64 times and the average spectra recorded. PEG coating concentration was estimated using thermogravimetric analysis (TGA). The TGA was carried out on a TA SDT Q600 (TA Instruments) with sequences of 20 °C/min ramp to 90 °C, isothermal for 10 min and 20 °C/min ramp to 600 °C.

Transmission electron microscopy

HNP suspensions (2 μL) were dried onto formvar coated copper grids. The grids were imaged using a JEOL JEM-1230 microscope (Jeol, Japan) using anaLYSIS software. Cellular internalisation images were taken after incubation of HNPs with BxPC-3 human pancreatic carcinoma and differentiated U937 human monocyte cells (acting as macrophage cells). Cells were grown into Aclar slides and incubated with HNP (25 μg mL^{-1}, 24 h). Cells were washed with PBS and fixed with 2.5 % gluteraldehyde in 0.1 M sodium cacoylate buffer: 2 mM calcium chloride (50:50) for 2 h. The samples were washed for 5 min in 0.1 M sodium cacodylate buffer: 2 mM calcium chloride, and this step was repeated a further two times. The samples were post fixed in 0.1 % osmium tetroxide in 0.1 M sodium cacodylate buffer/2 mM calcium chloride for 1 h. A series of dehydrations were carried out in ethanol before the samples were embedded in spurr resin. The samples were sectioned using a freshly cut diamond knife and placed onto formvar coated copper grids for imaging. The samples were imaged using a JEOL JEM-1230 microscope (Jeol, Japan) using anaLYSIS software.

Stability of HNPs

HNP solutions (10 mg mL^{-1}, previously reported (Barnett et al. 2012) were stored at room temperature in sealed vials for 6 months. The magnetic coercivity, size, zeta potential, T2 relaxivity and nano-heating capability were tested to determine whether, any degradation or physical changes had occurred since previous measurement. All measurements were carried out as previously reported (Barnett et al. 2012)

Stability of HNPs in physiological conditions

Test of stability in physiological conditions were carried out as previously reported (Hoskins et al. 2012b). Briefly, HNPs (both 'naked' and PEGylated, 100 μg mL^{-1}, 2 mL) suspended in deionised water were placed inside dialysis membrane with a molecular cut-off of 12–14 kDa and placed into conical flasks containing 200 mL RPMI cell culture media (Life Technologies, UK). Media was pH adjusted to pH 7.2 and 4.5 to mimic blood and lysosomal physiological conditions respectively. The system was sufficient to induce *in sink* condition. The particles were stirred over a 2 week period with sampling at 1, 4, 24, 48, 72, 168 and 336 h. The samples were analysed for Fe and Au content using inductively coupled plasma-optical emission spectroscopy (ICP-OES). Metal content in solution was calculated in respect to a calibration, and the percentage of the total Au content was deduced.

In vitro cellular assays

Cellular uptake of coated and uncoated HNPs

BxPC-3 and differentiated U937 cells were seeded into 6 well plates (50,000 cells/well) and incubated at 37 °C and 5 % CO_2. HNPs (both 'naked' and PEGylated, 25 μg mL^{-1}) were incubated with the cells for 24 h. Cells were washed with phosphate buffered saline (PBS) and trypsinised. Cells were resuspended (1,000,000 mL^{-1}) in fresh RPMI media (Life Technologies, UK). 1 mL of cell suspension was placed into an Eppendorf tube and centrifuged at 800 rpm for 10 min. The supernatant was discarded and the cells were resuspended in 1 mL concentrated nitric acid. The solutions were incubated at 90 °C for 1 h before dilution in deionised water. The iron (Fe) content was determined using ICP-OES and calculated per cell.

Cellular uptake mechanism via endocytosis inhibition study

Investigation into the mechanism of cellular internalisation of PEGylated HNPs was carried out by incubation of cells with nanoparticles (12.5 and 25 μg mL^{-1}) at 4 and 37 °C. Here serum free media was used as the particle diluent. Cellular uptake was deduced in terms of Fe content per cell as previously described.

Cell viability assay via trypan blue exclusion

BxPC-3 and differentiated U937 cells were seeded into 6 well plates (50,000 cells/well) and incubated for 24 h. HNPs were incubated with cells (6.25, 12.5, 25, 50 and 100 μg mL^{-1}) for 24, 48, 72 and 168 h* at 37 °C and 5 % CO_2. Cells were washed with PBS and trypsinised. Once detached cells were resuspended in 1 mL fresh media. Cell suspension (50 μL) was mixed with 50 μL trypan blue solution for 1 min. Cells were counted using a Countess® automated cell counter (Life Technologies, UK). Cell viability was determined in respect to control cells with no nanoparticles present.

For the 168 h time point, the cell culture media was changed after 72 h by removal of media, washing cells with PBS and addition of fresh media of the same nanoparticle concentration. This is in accordance with other cellular work reported in the literature, where media replacement is required (Hoskins et al. 2012b).

Cellular response assays

Cell membrane integrity, reactive oxygen species (ROS) and lipid peroxidation (LPO) assays were carried out on BxPC-3 and U937 cells incubated with HNPs (0–25 μg mL^{-1}). Protocols for these have been previously described (Hoskins et al. 2012b). Membrane integrity was measured via measurement of lactate dehydrogenase (LDH) leakage (Promega, UK) from BxPC-3 and differentiated U937 cells. Lactate dehydrogenase (LDH) levels were recorded at 560/590 nm, using a Tecan Pro200 microplate reader (Tecan, UK). The percentage of cytotoxicity was calculated in respect to control wells containing no nanoparticles. The degree of ROS was calculated as a percentage of DCF fluorescence in respect to control cells assumed to be 100 %. The fluorescence intensity of the samples was measured at 560 nm (excitation) and 590 nm (emission). The LPO levels were determined using the thiobarbituric acid reactive substance (TBARS) assay. The results were calculated as nmol of MDA/mg of cellular protein and compared with the levels in control cells. MDA levels and protein content were measured at 530 nm (excitation) and 550 nm (emission) and at absorbance of 595 nm respectively.

HNP-drug conjugate studies

Drug conjugation and quantification

Drug conjugation was carried out stirring 6-TG (25 mg) with the HNPs (5 mL, 5 mg mL^{-1}) at room temperature for 8 h. The particles were magnetically separated from solution and washed thoroughly with deionised water five times. The particles were resuspended in 5 mL deionised water to a final concentration of 5 mg mL^{-1} (Fe) which was confirmed using ICP-OES (data not shown). UV–Vis spectrometry was used to quantify the drug concentration conjugated to the particle surface (6-TG-HNP). The absorbance was measured at 330 nm on a UV-2600 UV–Vis(NIR) with an ISR-2600 Plus Integrated sphere (Shimadzu, Germany), and compared with a calibration curve ($R^2 = 0.999$). The concentration was worked out as a ratio in regards to 6-TG:Au:Fe. Hydrodynamic diameters and zeta potential measurements were carried out

as previously reported using a Zetasizer Nano-ZS (Malvern Instruments, UK) (Barnett et al. 2012).

Biological activity of 6-TG-HNP conjugates

The drug uptake and cell viability studies were carried out on BxPC-3 and differentiated U937 cells using 6-TG-HNP, compared with the free 6-TG drug and uncoated HNPs as a control. 6-TG concentration was worked out per cell after 4 h incubation with 12.5 and 50 μg mL^{-1} drug concentrations (and equivalent iron concentration for HNP controls). The cells were incubated with samples, followed by trypsinisation and counting as previously described. 6-TG concentration was determined using UV–Vis spectroscopy (see coating method). Cell viability studies were carried out using trypan blue exclusion (3.13–50 μg mL^{-1}) and the IC_{50} values estimated.

Results and discussion

Synthesis, PEGylation and characterisation of HNPs

Hybrid nanoparticles of 70 nm diameter were synthesised and characterised as described previously (Barnett et al. 2012). The HNPs were coated with a thiolated PEG through dative covalent bonding between the thiol moiety (–SH) on the polymer and the gold shell of the nanoparticles. FTIR spectroscopy confirmed the presence of characteristic peaks attributed to the PEG coating (Fig. 1) compared with the uncoated HNPs. These predominantly consisted of peaks arising from the C=O (1,340 cm^{-1}), C–O (1,466 and 1,101 cm^{-1}), and C–H (2,883 cm^{-1}) bonds respectively. Elemental analysis also confirmed the presence of C, H and N indicating that coating had been successful (Table 1). TGA analysis was used to quantify the PEG coating concentration in relation to 1 mg HNP core, the concentration was determined as 164 μg mL^{-1} (Table 1). TEM images of the uncoated and coated HNPs are shown in Fig. 2a1, a2 particle diameter was measured using the ANALysis software showed the average particle diameter to increase from 70 to 80 nm after PEGylation, indicating the coating thickness of the PEG was 5 nm (Fig. 2b1, b2).

Stability of uncoated hybrid nanoparticles

Table 2 shows the physical stability data of the HNPs (uncoated) previously reported (Barnett et al. 2012) after 6 months stored at room temperature in a 10 mg mL^{-1} solution. At this stage no surface modification had been made and hence, stability is based solely on the 70 nm HNPs. Particles were imaged using TEM in order to ascertain whether, morphology or diameter had changed as a result of the time period. Zeta potential was also measured, not as an indicator of particle monodispersity, but as an indicator of whether the gold shell had degraded or changed as a result of storage. Here, the data shows that no significant change in the average particle diameter was observed (255 nm, $p > 0.05$), compared with the freshly prepared particles previously reported (250 nm) (Barnett et al. 2012). This was confirmed with TEM microscopy, where the particle diameter remained constant (70 nm). Additionally, particle morphology appeared similar. An increase in polydispersity index was noted with the rise from 0.112 to 0.312 indicating that the particles may have started to form clusters, however, this was not apparent from the size data. Zeta potential measurements showed that the surface charge of the particles remained at +2.4 mV consistent with previous studies suggesting no degradation or complex formation had occurred. Magnetic coercivity (Hc) determined via SQUID measurement appeared to decrease from 10.35 kA m^{-1} (±5) to 6.2 kA m^{-1} (± 0.2) after 6 months (Table 2). This decrease in Hc suggests that the magnetic properties of the HNPs were modified over time. However, T_2 relaxivity remained relatively stable with comparable measurements (175.3 and 161.7 mM^{-1} s^{-1}, 0 and 6 months respectively). This suggested that the contrast ability of the HNPs was not affected over the duration of the study. Interestingly, the standard deviation in Hc measurement was larger in the initial measurement compared with the 6 months stability sample, however, it is not obvious if this is related. Finally, the agar suspended HNPs (10 μg mL^{-1}) were irradiated with a pulsed laser and their nano-heating ability determined. Here, the nanoparticles appeared to be stable after 6 months with comparable ΔT values to the initial study (Table 2). All the data indicated that these uncoated nanoparticles possessed similar physicochemical properties to the freshly made HNPs (Barnett et al.

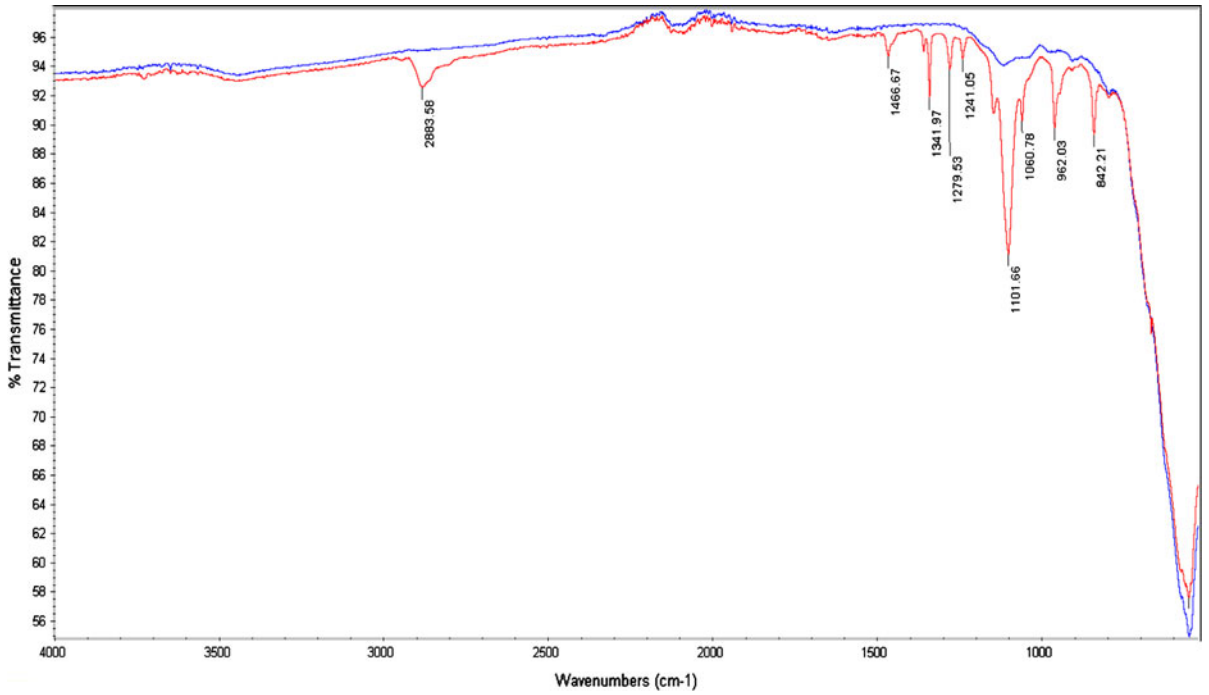

Fig. 1 FTIR analysis of uncoated and PEGylated HNPs. Analysis carried out on freeze dried samples using a diamond tip ATR attachment (no. scans = 64)

Table 1 Chemical analysis of PEGylated hybrid nanoparticles

Analytical method	Measurement		Result
Elemental analysis	Relative abundance, wt/wt	C	0.87
		H	0.14
		N	0.05
Thermogravic analysis	Weight of PEG per 1 mg HNP, μg mL^{-1}		164

2012). Hence, we can conclude that no major structural degradation had occurred and the HNP integral structure was stable over this time period.

Chemical stability of coated and uncoated HNPs

Chemical stability of the HNPs at physiological pH was determined over a 2 week period in order to give an appreciation of the degradation, which may occur after in vitro and in vivo application. The particles were stirred in dialysis membrane surrounded by cell culture media of pH 7.2 to mimic physiological, and pH 4.6 to mimic intracellular lysosomal conditions. The % of initial Fe and Au content were determined via ICP-OES analysis. An increase in metal content outside the dialysis chamber is indicative of particle degradation. This technique is highly sensitive and hence, metal content can be detected at extremely low quantities in solution. Figure 3 shows the degradation curves for Au in (A) uncoated and (B) PEGylated HNPs. The data for Fe degradation is not shown as no measureable degradation was observed which is reasonable, given, the rigid nature of the gold coating. In both coated and uncoated HNPs an initial burst of Au into the surrounding media was observed followed by a plateau in degradation over the study period. This could be due to some excess gold nanoparticulate impurities remaining in solution after purification; however, the levels are so low these are classed as negligible. After 2 weeks only 0.007 % of initial Au was observed in the media at pH 7 and 0.008 % at pH 4.6. The increase in Au at lower pH is rational, given that the solubility of gold increases in acidic environments, however, this theory requires some further exploration. In any case, for this study the low gold concentrations indicate that particle integrity was not compromised. After PEGylation (Fig. 3b) the amount of Au present after 2 weeks in the surrounding media was reduced to 0.0015 % (pH 7) and 0.0045 % (pH

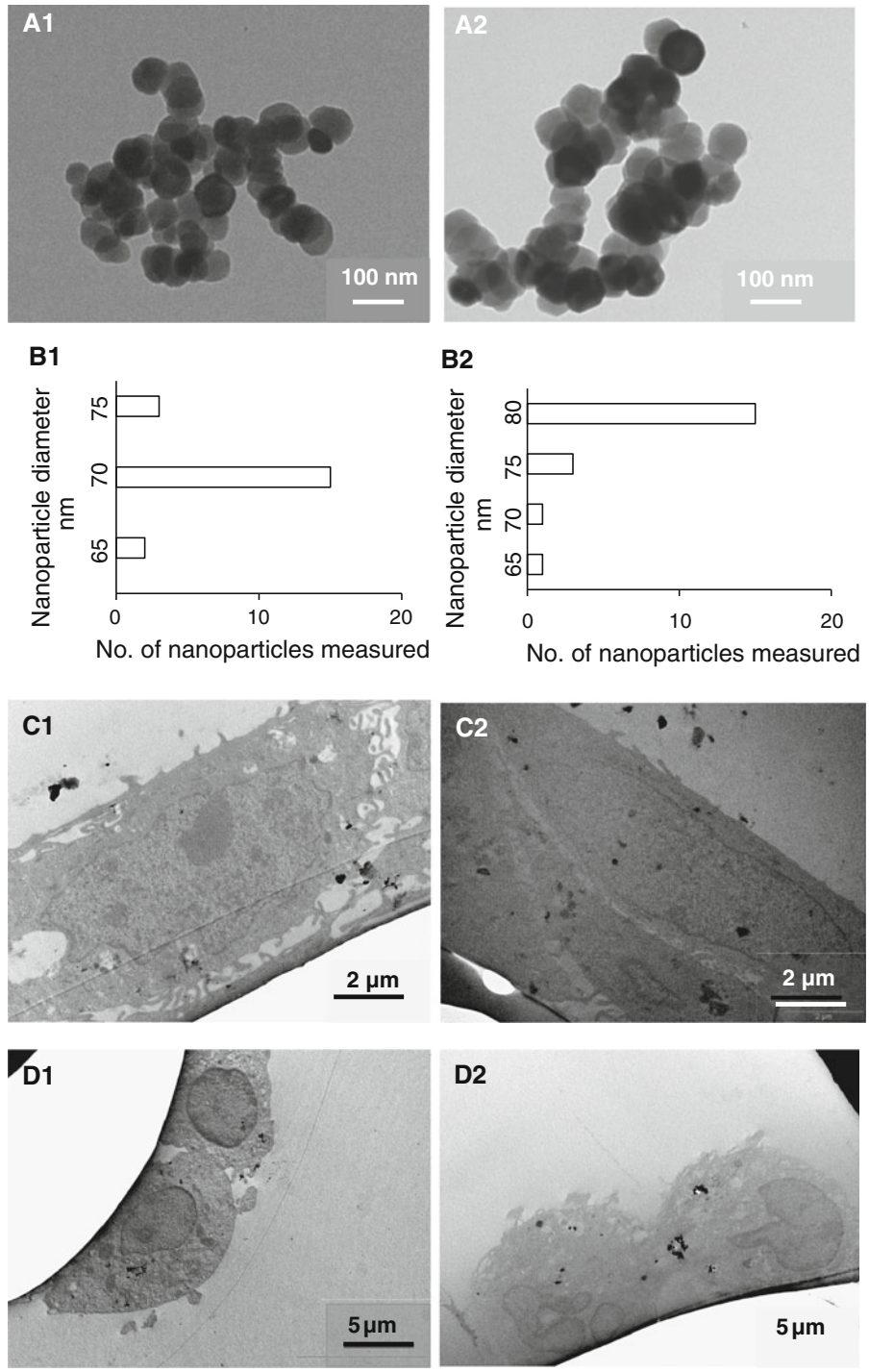

Fig. 2 TEM images of nanoparticles **a1** HNP, **a2** HNP-PEG, and **b** their corresponding size distribution as measured by the ANALysis software ($n = 20$). Cellular uptake of nanoparticles in **c** BxPC-3 and **d** U937 cells (*1* and *2* HNP and HNP-PEG respectively)

4.6). Hence, after polymer coating of the HNPs with PEG a greater degree of shielding from degradation was achieved. The negligible media Fe content observed in this experiment (data not shown) further confirms that particle integrity was maintained across the study, thus no Fe could be released.

Table 2 Physical stability of HNPs over 6 months stored in solution at room temperature ($n = 3 \pm$ SD)

Physical property	0 months[a]	6 months
Size using photon correlation spectroscopy, nm	250 (22)	255 (62)
Polydipersity index	0.112 (0.010)	0.312 (0.021)
Zeta potential, mV	+2.4 (0.00)	+2.4 (0.01)
Size from transmission electron microscopy, nm	70 (0.5)	70 (0.4)
Magnetic coercivity from SQUID measurement, kAm^{-1}	10.35 (5)	6.2 (0.2)
T2 relaxivity from MRI measurement, $mM^{-1}\ s^{-1}$	175.3 (1)	161.7 (7.3)
ΔT from laser irradiation of 10 μg mL^{-1} suspended in 2 % agar, °C	7.0 (0.5)	7.5 (0.8)

[a] Data previously described [6]

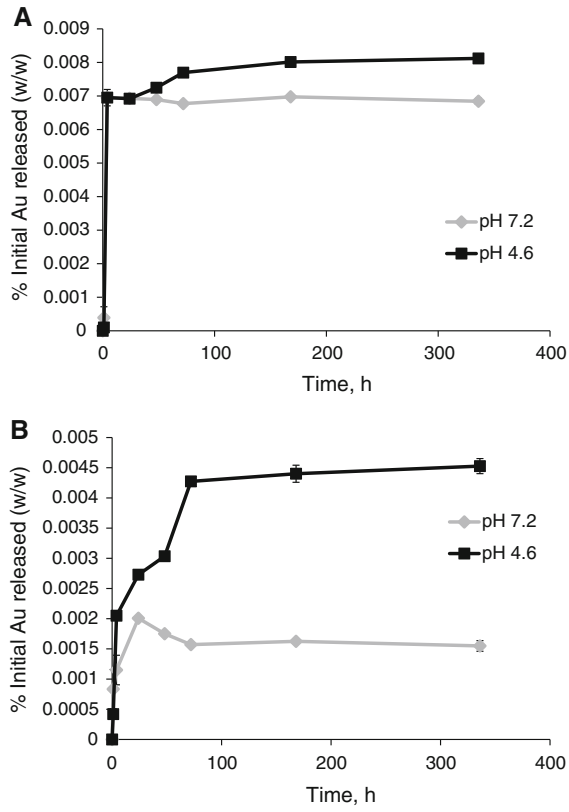

Fig. 3 Stability of HNPs in solution under in biological conditions at pH 7.2 and 4.6. **a** HNP and **b** HNP-PEG. Study carried out under *in sink* conditions over 2 week period and % initial Au determined ($n = 3 \pm$ SD)

In vitro cellular assays

Cellular uptake studies were carried out on BxPC-3 and differentiated U937 cells incubated with both uncoated and PEGylated HNPs (25 μg mL^{-1}) for 24 h. Differentiated U937 cells exhibit macrophage like activity and hence, these two cell lines were used in order to demonstrate cellular activity in both tumour and immune system environments. Both experiments were carried out in serum free media, in order to prevent protein complexation onto the HNP surface. Zeta potential measurements of the HNP suspensions in media showed no electrolyte complexation had occurred prior to incubation (data not shown). Figure 4 shows the total iron concentration per cell. After incubation with the uncoated HNPs, the intracellular iron concentration in BxPC-3 cells increased almost 10-fold from 0.109 pg (with no HNPs present) to 1.01 pg. A similar trend was observed in U937 cells incubated with the uncoated HNPs where a 5-fold increase in Fe concentration compared with basal levels was measured. After PEGylation, the intracellular Fe concentration was significantly increased ($p < 0.05$) compared with basal levels and with Fe levels in the cells incubated with the uncoated HNPs. Here, concentrations as high as 7.56 and 4.70 pg were observed in the BxPC-3 and U937 cells, respectively. This study further highlights that surface functionalization is crucial in order for increased biological interactions to occur. Here, the presence of the PEG molecule on the surface of the HNPs promoted cellular internalisation. Interestingly, increased Fe content was observed in the BxPC-3 cells compared with the U937. This could be due to the rapidly proliferating rate of the tumour cell line experiencing greater cellular internalisation compared with the macrophage like cells. Generally, it would be expected that macrophage cell lines experience increased cellular internalisation due to their phagocytotic and endocytotic nature, however, the cell line used in this study are human monocyte cells (U937) which require differentiation in order to achieve their macrophage-like qualities. It has been well documented that although these behave in a similar manner to macrophage cells, after differentiation a large decrease in cell proliferation occurs (Hosoya and Marunouchi 1992). TEM images (Fig. 2c, d) show nanoparticle presence was observed in cells containing the both the HNP and HNP-PEG in

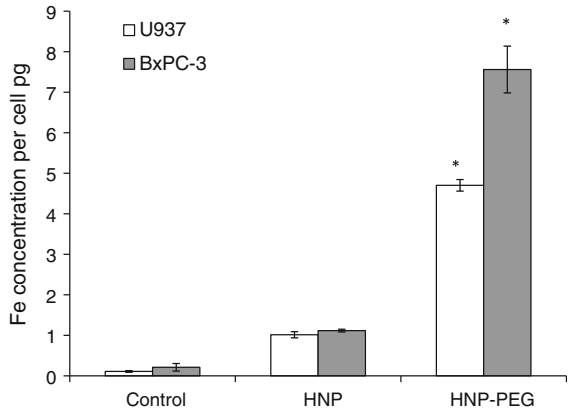

Fig. 4 Cellular uptake of Fe into BxPC-3 and U937 cells after 24 h incubation with 25 μg mL^{-1} HNP and peglyated HNP's ($n = 3 \pm$ SD). * Denotes significant difference compared with control ($p < 0.05$)

both cell lines, although, no difference in uptake levels between the coated and uncoated was observed.

A subsequent study was carried out using only the HNP-PEG (12.5 and 25 μg mL^{-1}) in order to determine their cellular uptake mechanism. Theoretically, endocytosis will be inhibited at 4 °C. This is because endocytosis is a process which is energy dependent. At lower temperatures, cellular energy is decreased and inhibition of uptake by endocytosis occurs. Other routes of cellular uptake such as passive diffusion are not energy dependent hence, these should still occur at low temperatures (Majumdar et al. 2009). Table 3 shows the concentration of intracellular Fe after 1 and 4 h incubation at 4 and 37 °C. At 12.5 μg mL^{-1} the cellular uptake appeared to be temperature and time dependent. In the BxPC-3 cells a 1.9-fold increase in Fe concentration was observed at 37 °C compared with 4 °C after 1 h. After 4 h incubation a 2-fold increase was observed. A similar trend was observed in the U937 cells, where a 1.5-fold increase occurred after 1 h and 2.2-fold increase after 4 h in the cells incubated at 37 °C compared with the lower temperature. None of these values were found to be significant ($p > 0.05$). This data suggests that endocytosis may play a role in cellular uptake of the HNPs, however, this does not appear to be the only uptake route. Interestingly, at the higher HNP concentration (25 μg mL^{-1}) no obvious trend was observed in HNP uptake in the samples incubated at 4 and 37 °C with regard to uptake by endocytosis. Cellular uptake mechanisms are complex and small changes in temperature can induce in misguided conclusions, hence, more work is being carried out in this field using endocytosis inhibitors (such as sodium azide), in order to fully elucidate the mechanisms involved in HNP uptake.

Cell viability was estimated using BxPC-3 (Fig. 5a1) and differentiated U937 (Fig. 5a2) cells incubated with HNP-PEG (6.25–100 μg mL^{-1}). The data shows that the PEGylated HNPs did not possess any undesirable cytotoxicity over the concentration range within the duration of this study (3 days). The cell membrane integrity assays (Fig. 5b1, b2) indicated that the presence of the HNP-PEG did not result in increased LDH formation compared with basal levels. Hence, the nanoparticles showed no adverse effect on the integrity of the cell membrane in either cell line. Similarly, the ROS and LPO data did not show any increase in free radical production due to singlet oxygen (Fig. 6a1, a2) or lipid peroxidase (Fig. 6b1, b2) compared with the control cells. When looking at the TEM cellular uptake (Fig. 2c, d) and Fe content assays (Figs. 3, 4) it is evident that these nanoparticles are entering the cell, hence, these results are highly promising. This data is in good agreement with the chemical stability studies where no quantifiable levels of Fe were detected. It is hypothesized that after cellular uptake, iron oxide nanoparticles are degraded via enzymatic hydrolysis into iron ions (Shubayev et al. 2009). The reactive oxygen species induced by transition metal particle degradation can then result in lipid peroxidation (Sorensen et al. 2003, Zhu et al. 2008). Lipid peroxidation causes intracellular stresses from hydrogen peroxide generation, and causes disruption of the phospholipid bilayer which can result in cell death (Minotti and Aust 1987). This data further highlights, the benefit of the added rigid gold coating surrounding the iron oxide core which results in a highly biocompatible HNP construct.

HNP-drug conjugate studies

In this study, the potential of the HNPs to act as drug carriers was also evaluated. 6-TG was used as a model drug and conjugated via dative covalent bonding between the thiol (–SH) group on the drug molecule and the Au nano-shell surface. The HNP-6-TG attachment was verified using UV–Vis spectroscopy. The 6-TG possessed a large absorbance value at 330 nm (Fig. 7), a peak was also observed at 650 nm

Table 3 Cellular uptake of PEGylated HNPs (12.5 and 25 μg mL^{-1}) in BxPC-3 and differentiated U937 cells incubated at 4 and 37 °C over 1 and 4 h ($n = 3 \pm$ SD)

Particle	Concentration of Fe per cell, pg (± SE)			
	4 °C		37 °C	
	1 h	4 h	1 h	4 h
BxPC-3				
Control	0.137 (0.032)	0.069 (0.014)	0.116 (0.072)	0.084 (0.013)
12.5	0.932 (0.143)	1.199 (0.171)	1.738 (0.280)	2.459 (0.178)
25	6.705 (0.903)	7.331 (1.561)	6.685 (0.555)	7.741 (0.704)
U937				
Control	0.060 (0.011)	0.0635 (0.008)	0.0637 (0.011)	0.0552 (0.001)
12.5	1.286 (0.302)	0.907 (0.146)	1.892 (0.162)	1.954 (0.148)
25	5.280 (0.681)	6.018 (0.350)	3.972 (0.643)	5.905 (0.454)

due to the plasmon resonance of the gold coat as discussed previously (Barnett et al. 2012). Here, we observed a peak shift in the gold spectrum from 690 nm, previously reported to 650 nm (Barnett et al. 2012), whereas, the λ_{max} for the drug remained unchanged. Hydrodynamic diameter measurement (270 nm) and zeta potential measurement (+9.2 mV) also confirmed drug attachment compared with the uncoated HNPs (250 nm, +2.4 mV respectively). The 6-TG concentration conjugated to the HNP surface was calculated to be in a 3:1:10 ratio for Fe:Au:6-TG (wt:wt:wt) using both ICP-OES and UV–Vis spectrometry, respectively.

In order to determine whether the HNP drug carriers could promote cellular drug uptake, the HNP-6-TG conjugates were incubated both with BxPC-3 and differentiated U937 cells (12.5 and 50 μg mL^{-1}). At 12.5 and 50 μg mL^{-1} drug concentration, 3.75 and 15 μg mL^{-1} of Fe and 1.25 and 5 μg mL^{-1} Au were present, respectively. These values were relatively low and no toxicity was observed at these concentrations in the previous studies. After 4 h the 6-TG uptake per cell was estimated (Fig. 8a1, a2). The data showed consistently that increased 6-TG uptake was observed in the cells incubated with the HNP-drug conjugates compared with the free drug. At 50 μg mL^{-1}, the 6-TG concentration was 35-fold and 21-fold higher for the HNP-6TG compared with the free drug in the BxPC-3 and U937 cells, respectively ($p < 0.05$). The uncoated hybrids showed negligible 6-TG uptake as expected

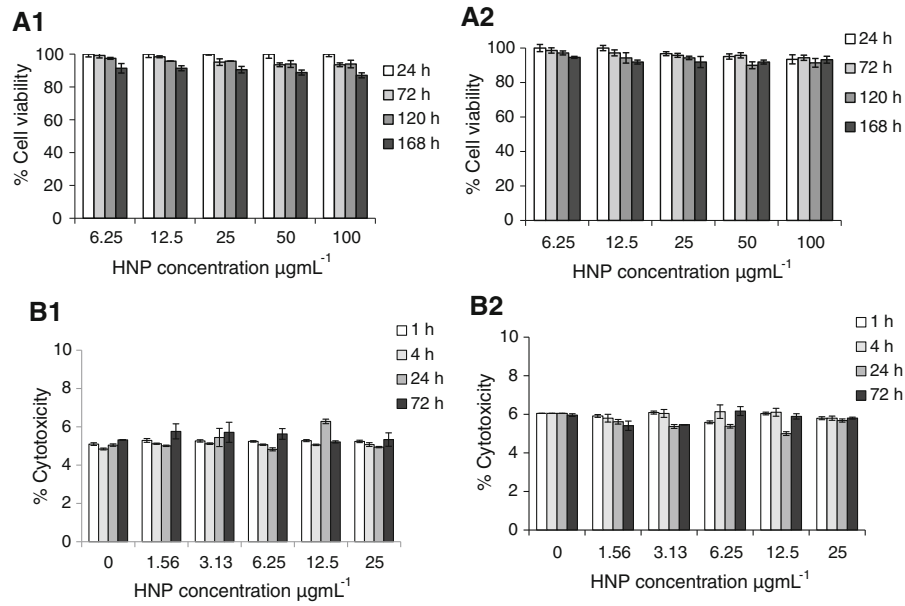

Fig. 5 Cellular response to pegylated HNP exposure via **a** cytotoxicity evaluated using trypan blue exclusion and **b** cell membrane integrity measured via LDH leakage. Assays carried out on *1* BxPC-3 and *2* Differentiated U937 cells. ($n = 3 \pm$ SD)

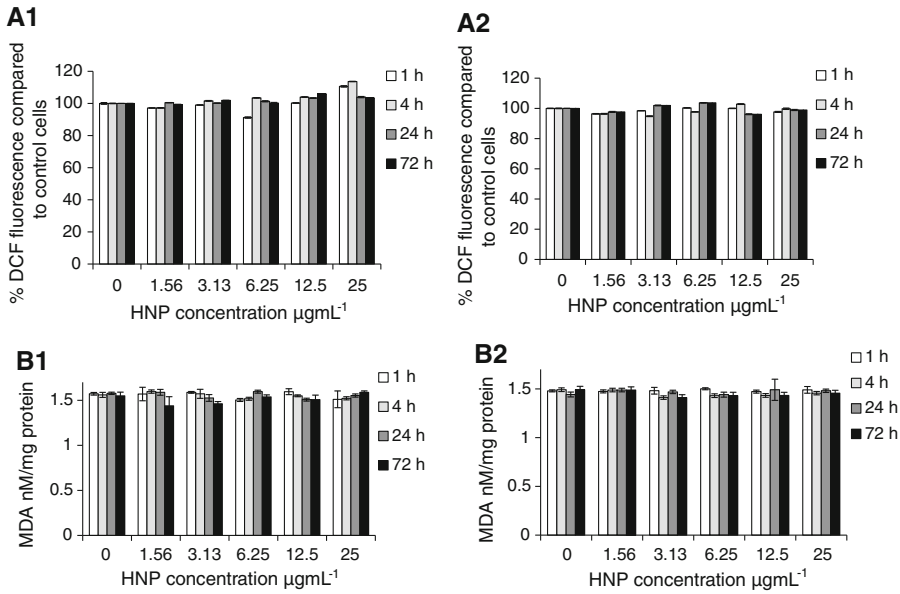

Fig. 6 Cellular response to pegylated HNP exposure via **a** reactive oxygen species (ROS) and **b** lipid peroxidation generation. Assays carried out on *1* BxPC-3 and *2* Differentiated U937 cells. ($n = 3 \pm$ SD)

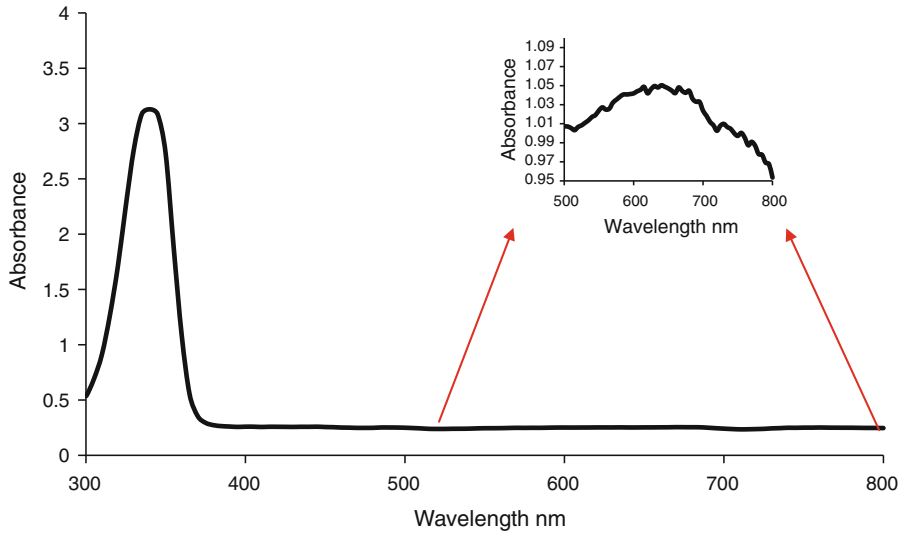

Fig. 7 Representative UV absorption spectra of 6-TG conjugated hybrid nanoparticle showing characteristic absorption peak of 6-TG at 330 nm and Au at 650 nm

due to their poor surface qualities, in line with previous HNP-PEG cellular uptake studies. These exciting findings suggest that once conjugated to hybrid nanoparticles, greater cell penetration occurs. This was particularly the case in the BxPC-3 tumour cells. Thus, increased drug uptake of the 6-TG could result in reduced dosage concentrations being required for similar therapeutic effect and hence, reduce patient side effects. Additionally, a reduction in treatment costs would ensue. This is a follow on study to elucidate the potential of the HNPs for drug carriers (the 6-TG formulation again is only a preliminary proof of concept study, the authors are not suggesting this is the ideal formulation).

Little work has been carried out on the cellular uptake of drugs bound to HNPs. However, previous studies have reported the use of nano-sized graft amphiphilic polymers (Poly(allylamine)-g-cholesterol) for encapsulation and delivery of a novel drug for pancreatic cancer (bisnaphtalamidopropyldiaminooctane, BNIPDaoct) (Hoskins et al. 2010). Here, the polymer nano-aggregates formed were passively targeted to tumour tissue. The formulation was administered in vivo in a pancreatic cancer model using nude

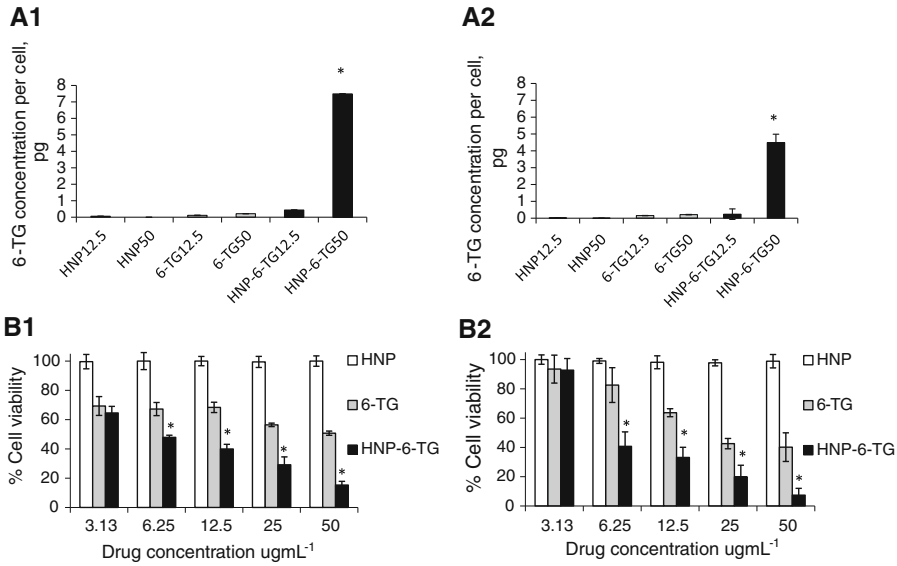

Fig. 8 Biological studies on **a** drug uptake of 6-TG after 4 h (12.5 and 50 μg mL^{-1}) incubation and **b** cell viability by trypan blue exclusion after 24 h HNP incubation on *1* BxPC-3 and *2* differentiated U937 cells ($n = 3 \pm$ SD). * Denotes significant difference compared with free drug levels ($p < 0.05$)

tumour bearing mice over a period of 4 weeks. Although the BNIPDaoct dose was eight-fold less than clinically used gemcitabine, the formulation was able to reduce tumour growth in xenograft mice with comparable results (Hoskins et al. 2010). Here, the ability of the nano-formulation to passively target the pancreatic cancer tumour was observed. Although this study uses a different carrier vehicle with differing structural and surface properties, it could serve as a starting point highlighting the ability of nanoparticulates to passively target tumour tissue.

The ability of the HNP-drug conjugates to act as cytotoxic agents was evaluated over 24 h period. Although 6-TG is currently used clinically as an antitumour agent in the treatment of leukaemia, its potential use after permanent conjugation to HNPs has not been explored in pancreatic cancer. After 24 h incubation of drug conjugates (50 μg mL^{-1}) a large decrease in cell viability was observed (80 % reduction) compared with the free drug (55 %) reduction (Fig. 8b1). The IC_{50} also decreased 10-fold from 50 μg mL^{-1} (with the free 6-TG) to 5 μg mL^{-1} with the HNP-6TG. These results are in agreement with the drug uptake studies whereby, increased drug uptake was observed when the 6-TG was conjugated to the HNP in comparison with the free drug. The U937 cells showed a similar trend (Fig. 8b2). This data shows that the cytotoxic integrity of the 6-TG is not impeded by conjugation via the thiol dative linkage. This study was also in agreement with findings by Wagstaff et al. (2012) who conjugated cytotoxic agent cisplatin onto HNPs. They found that after incubation with human ovarian carcimons (A2780) cells, their novel formulation was up to 110-fold more cytotoxic than the free drug (Wagstaff et al. 2012).

Although 6-TG is clinically used to treat leukaemia, its use has diminished in recent years due to the large array of side effects resulting from patient administration (Katsanos and Tsianos 2010). These include conditions such as ulcerative colitis, and bone marrow toxicity (Katsanos and Tsianos 2010). The main advantages of nanotechnology are the ease of synthesis, functionalization and sterilisation, along with the ability to passively target tumour cells. This is achieved via the enhanced permeability and retention (EPR) effect (Lyer et al. 2006). The EPR effect also reduces the concentrations of drug in the systematic circulation, hence, reducing exposure and toxic or undesirable side effects. Further study is being carried out in this area in order to decipher whether, conjugation to the HNP the 6-TG would exhibit preferential accumulation in tumour tissue using common in vivo pancreatic cancer models.

Conclusions

The potential use of HNPs in image-guided therapies is rapidly being realised. However, three main factors need to be addressed to deem these nanoparticles

suitable for biological application. The importance and implications of HNP (1) stability and (2) toxicity has not yet been fully reported. Here, we showed that the physical properties of the HNPs were largely unaffected after 6 months storage in aqueous solution at room temperature. The data showed no major deviation from our initial study (Barnett et al. 2012). The structural integrity of the HNPs was not compromised after stirring in solutions designed to mimic physiological pH. This observation is hugely important as degradation of the iron oxide core can lead to free radical production resulting in cell stress and subsequent morbidity. In agreement with this data, no free radical (ROS or LPO) production was observed above basal levels after 72 h incubation with both BxPC-3 and differentiated U937 cells. Additionally, no significant cytotoxic response was observed in cells incubated with the particles at concentrations as high as 100 μg mL^{-1} for up to 1 week.

Studies of the ability of these particles to carry pharmaceutical cargo such as drug molecules, genes, targeting ligands, etc. are beginning to emerge. Here, we conjugated the anticancer drug 6-TG onto the HNP surface through permanent thiol-gold dative covalent bonding in a ratio of 3:1:10 (Fe:Au:6-TG, wt:wt:wt). The novel formulation was incubated in vitro and total drug uptake per cell determined. The study showed that the cells incubated with HNP-6-TG experienced increased drug uptake concentrations compared with the free 6-TG indicating that the HNPs promote cellular internalisation. This was observed in both cell lines; however, in the BxPC-3 tumour cells greater intracellular drug concentrations were observed compared with the macrophage-like differentiated U937 cells. This can be attributed to the increased rate of proliferation of the tumour cells (BxPC-3).

The additional physical properties of the HNPs; such as their image-guided capabilities or thermal manipulation through laser irradiation adds further benefit to this class of drug carrier. Ultimately, these novel carriers can be further functionalised to achieve active targeting and stimuli-responsive drug release by external triggers such as heat via laser irradiation. This preliminary study shows that an exciting future lies ahead for the use of HNPs as multifunctional drug delivery vehicles. Further in vivo studies are being carried out in order to investigate whether enhanced permeation into the cancerous tissues occurs. This increased internalisation results in decreased dosages and thus, higher drug efficacy. Furthermore, this could ultimately reduce side effects of toxic drugs, such as those experienced by patients prescribed 6-TG.

Acknowledgments This study was financially supported by the School of Pharmacy and the Institute of Science and Technology, Keele University. ICP studies were carried out in the School of Physical and Geographical Sciences, Keele University. The authors wish to thank Dr. Paul Roach and Dr. Ying Yang for the use of the TGA at the Institute of Science and Technology for Medicine. All MRI measurements were carried out in Professor Andreas Melzer's laboratory in Institute of Medical Science and Technology, University of Dundee. The magnetometer used in this research was obtained through the Science City Advanced Materials project: Creating and Characterizing Next Generation Advanced Materials project, with support from Advantage West Midlands (AWM) and part funded by the European Regional Development Fund (ERDF).

References

Albanese A, Tang PS, Chan WCW (2012) The effect of nanoparticle size, shape and surface chemistry on biological systems. Annu Rev Biomed Eng 14:1–16

Arruebo M, Fernández-Pacheco R, Ibarra R (2007) Magnetic nanoparticles for drug delivery. Nano Today 2:22–32

Barnett CM, Gueorguieva M, Lees MR, McGarvey DJ, Darton RJ, Hoskins C (2012) Effect of the hybrid composition on the physicochemical properties and morphology of iron oxide–gold nanoparticles. J Nanopart Res 14:1170

Buzea C, Pacheco B II, Robbie K (2007) Nanomaterials and nanoparticles: sources and toxicity. Biointerphases 2: MR17–MR172

Chatterjee S, Bandyopadhyay A, Sarkar K (2011) Effect of iron oxide and gold nanoparticles on bacterial growth leading towards biological application. J Nanobiotechnol 9:34

Dobson J (2006) Magnetic nanoparticles for drug delivery. Drug Dev Res 67:55–60

Fadeel B, Garcia-Bennett AE (2010) Better safe than sorry: understanding the toxicological properties of inorganic nanoparticles manufactured for biomedical applications. Adv Drug Deliv Rev 62:362–374

Hoskins C, Ouaissi M, Lima SC, Cheng WP, Loureirio I, Mas E, Lombardo D, Cordeiro-sa-Silva A, Ouaissi A, Kong Thoo Lin P (2010) The study of in vitro and in vivo anticancer activity of a novel formulation incorporating PAA and BNIPDaoct against pancreatic cancer. Pharmaceut Res 27:2694–2703

Hoskins C, Min Y, Gueorguieva M, McDougall C, Volovick A, Prentice P, Wang Z, Melzer A, Cuschieri A, Wang L (2012a) Hybrid gold–iron oxide nanoparticles as a multifunctional platform for biomedical application. J Nanobiotechnol 10:27

Hoskins C, Wang L, Cuschieri A (2012b) The cytotoxicity of polycationic nanoparticles: common endpoint assays and alternative approaches for improved understanding of cellular response mechanism. J Nanobiotechnol 10:15

Hosoya H, Marunouchi T (1992) Differentiation and dedifferentiation of the human monocytic leukemia cell line, U937. Cell Strct Funct 17:263–269

Ji X, Shao R, Elliott AM, Stafford J, Esparza-Coss E, Bankson JA, Liang G, Luo Z-P, Park K, Markert J-T, Li C (2007) Bifunctional gold nanoshells with a superparamagnetic iron oxide: silica core suitable for both MR Imaging and photothermal therapy. J Phys Chem C 111:6245–6251

Józejczak A, Skumiel A (2011) Ultrasonic investigation of magnetic nanoparticles suspension with PEG biocompatible coating. J Magn Magn Mater 11:1509–1516

Katsanos K, Tsianos EV (2010) Non-TPMT determiniants of azathioprine toxicity in imflammatory bowel disease. Ann Gastroenterol 23:95–101

Lancaster DL, Patel N, Lennard L, Lilleyman JS (2001) 6-Thioguanine in children with acute lymphoblastic leukaemia: influence of food on parent drug pharmacokinetics and 6-thioguanine nucleotide concentrations. BJCP 56:531–539

Lu A-H, Salabas EL, Schüth F (2007) Magnetic nanoparticles: synthesis, protection, functionalization, and application. Angew Chem Int Ed 46:1222–1244

Lyer AK, Khaled G, Fang J, Maeda H (2006) Exploiting the enhanced permeability and retention effect for tumor targeting. Drug Discov Today 11:812–818

Majumdar S, Tejo BA, Badawi AH, Moore D, Krise JP, Siahaan TJ (2009) Effect of modification of the physicochemical properties if ICAM-1-derived peptides on internalization and intracellular distribution in the human leukemic cell line HL-60. Mol Pharm 6:396–406

Manson J, Kumar D, Meenan BJ, Dixon D (2011) Polyethylene glycol functionalized gold nanoparticles: the influence of capping density on stability in various media. Gold Bull 4:99–105

Minotti G, Aust SD (1987) The requirement for Iron(III) in the initiation of lipid peroxidation by Iron(II) and hydrogen peroxide. J Biol Chem 262:1098–1104

Mishra S, Webster P, Davis ME (2004) PEGylation significantly affects cellular uptake and intracellular trafficking of non-viral gene delivery particles. Eur J Cell Biol 83:97–111

Peng J, Zou F, Liu L, Tang L, Yu L, Chen W, Liu H, Tang Jb Wu (2008) Preparation and characterization of PEG-PEI/Fe_3O_4 nano-magnetic fluid by co-precipitation method. Trans Nonferrous Met Soc China 18:393–398

Shubayev VI, Pisanic TR, Jun S (2009) Magnetic nanoparticles for theragnostics. Adv Drug Deliv Rev 61:467–477

Sorensen M, Autrup H, Moller P, Hertel O, Jensen SS, Vinzents P, Knudsen LE, Loft S (2003) Linking exposure to environmental pollutants with biological effects. Mutat Res 544:255–271

Sun C, Lee JSH, Zhang M (2008) Magnetic nanoparticles in MR imaging and drug delivery. Adv Drug Deliv Rev 60: 1252–1265

Vila A, Gill H, McCallion O, Alonso MJ (2004) Transport of PLA-PEG particles across the nasal mucosa: effect of particle size and PEG coating density. J Control Release 98:231–244

Wagstaff AJ, Brown SD, Holden MR, Craig GE, Plumb JA, Brown RE, Schreiter N, Chrzanowski W, Wheate NJ (2012) Cisplatin drug delivery using gold-coated iron oxide nanoparticles for enhanced tumour targeting with external magnetic fields. Inorg Chim Acta 393:328–333

Zaza G, Cheok M, Krynetskaia N, Thorn C, Stocco G, Hebert JM, McLeod H, Weinshilbourn RM, Relling MV, Evans WE, Klein TE, Altman RB (2010) Thiopurine pathway. Pharmacogenet Genomics 20:573–574

Zhu M-T, Feng W-Y, Wang B, Wang T-C, Gu Y-Q, Wang M, Wang Y, Ouyang H, Zhao Y-L, Chai Z-F (2008) Comparative study of pulmonary responses to nano- and submicron sized ferric oxide in rats. Toxicology 247:102–111